Nanoscale Advances

ROYAL SOCIETY OF CHEMISTRY

PAPER

View Article Online
View Journal | View Issue

Cite this: *Nanoscale Adv.*, 2021, **3**, 3100

Theoretical study of the influence of doped oxygen group elements on the properties of organic semiconductors†

Anmin Liu, *[a] Mengfan Gao,[a] Yan Ma,*[ae] Xuefeng Ren, *[b] Liguo Gao,[a] Yanqiang Li[a] and Tingli Ma[cd]

Received 6th December 2020
Accepted 6th April 2021

DOI: 10.1039/d0na01026j

rsc.li/nanoscale-advances

Organic semiconductor materials are widely used in the field of organic electronic devices due to their wide variety, low price, and light weight. However, their developments are still restrained by their low stability and carrier mobility. Density functional theory (DFT) was used to study the influence of doped oxygen group elements (O, S, Se, and Te) on the properties of organic semiconductor materials (seven-membered benzothiophene, *o*-pentacene, thiophene derivatives, and pentacene) in this paper. Based on the calculation of E_{HOMO}, E_{LUMO}, ΔE, and total energy, the performances of organic semiconductor materials without and with doped elements were compared, and it was found that the doping of multi-element Te makes the material have high stability and potential high mobility. For these studied organic semiconductor materials, when the atoms of the doped site change in the order of O, S, Se, and Te, the carrier mobility gradually increases, and the molecules show a tendency of stability. In this paper, promising doping elements and doping methods for these studied molecules are determined through calculations and screening out suitable materials more efficiently and economically without a large amount of repetitive experimental work, which may provide a theoretical basis and guidance for preparing high-performance organic semiconductor materials.

1. Introduction

In the past few decades, organic semiconductors have attracted the attention of many researchers due to their adjustable electronic structure and optical band gap, light weight, and good mechanical flexibility.[1–3] Because of their favorable performance, a large number of organic materials have been widely designed and applied in the fields of organic light-emitting diodes,[4,5] organic thin film transistors,[6] and organic solar cells.[7] Compared with inorganic semiconductors, organic semiconductors possess discrete "energy levels" composed of molecular orbitals, and the transfer of charge depends on the ability of carriers to move from one molecule to another.[5] Carrier mobility is one of the important indicators for evaluating the performance of organic semiconductors.[8] The higher the carrier mobility rate, the better the performance of the prepared device.[9,10]

Improving carrier mobility is the key to the development of organic semiconductor materials. In the past few decades, researchers have made significant progress in enhancing the carrier mobility of organic semiconductors.[11–16] Appropriate molecular design and doping can adjust conductivity and make organic semiconductors potentially useful.[17–20] Doping, especially with oxygen group elements,[21–26] can lead to the formation of more free charge carriers in organic semiconductors or the passivation of traps, increase carrier mobility, increase the effective injection of electrons, change charge transport properties, and improve the carrier mobility and stability of the material. Di Tian[27] *et al.* introduced polarizable and electron-rich sulfur or selenium atoms into electron-deficient nitrogen-containing heteroaromatic compounds, which facilitated the accumulation of adjacent molecules and achieved a π-atom orbital overlap rate of more than 90%.

Common organic semiconductor materials include polycyclic aromatic hydrocarbons (PAHs), metal complexes and small compounds derived from conductive polymers, such as polyolefins, polythiophenes, and pentacene.[28–33] The molecular structure and semiconductor properties of these materials have been a hot spot in recent years. Among them, in organic light-

[a]State Key Laboratory of Fine Chemicals, School of Chemical Engineering, Dalian University of Technology, China. E-mail: liuanmin@dlut.edu.cn; anmin0127@163.com

[b]School of Ocean Science and Technology, Dalian University of Technology, Panjin, 124221, China. E-mail: renxuefeng@dlut.edu.cn

[c]Department of Materials Science and Engineering, China Jiliang University, Hangzhou, 310018, China

[d]Graduate School of Life Science and Systems Engineering, Kyushu Institute of Technology, 2-4 Hibikino, Wakamatsu, Kitakyushu, Fukuoka 808-0196, Japan

[e]School of Economics and Finance, Xi'an Jiaotong University, China. E-mail: 18304280768@163.com

† Electronic supplementary information (ESI) available. See DOI: 10.1039/d0na01026j

emitting devices, the mobility of organic semiconductors based on thiophene and oligoacene is higher than 1.0 $cm^2 V^{-1} s^{-1}$,[34,35] and thiophene derivatives have excellent stability and high carrier mobility on linear oligoacetylene,[36] making them common semiconductor materials.

In this paper, we used density functional theory (DFT) to explore the effects of doping oxygen group elements on the conductivity and stability of organic semiconductor materials (seven-membered benzothiophene, *o*-pentacene, thiophene derivatives, and pentacene), and calculate the highest occupied molecular orbital (HOMO) and lowest unoccupied molecular orbital (LUMO) of a molecule (corresponding to the valence band and conduction band of the semiconductor[37]), and the smaller the difference between LUMO and HOMO, the easier the electronic transition between the orbitals.[38] By comparing the values of ΔE, total energy and other data, we get the general law of doping oxygen group elements, which provides guidance for screening high-performance organic semiconductor materials.

2. Computational methods

Geometry optimization, electronic properties, and orbital information of organic semiconductor materials were studied by the density functional theory (DFT) method using the DMol3 module in Materials Studio. The generalized gradient approximation (GGA) was treated by the Perdew–Burke–Ernzerhof (PBE) functional. The double numerical atomic orbital plus polarization function (DNP) of basfile v4.4 was chosen to be the basis set. The convergence criteria for the total energy calculation and geometric optimization step were set as below: a self-consistent field (SCF) energy tolerance of 10^{-5} eV per atom, a maximum force tolerance of 10^{-1} eV $Å^{-1}$, and a maximum displacement tolerance of 5×10^{-3} Å. Max self-consistent field cycles were set as 1000 cycles.

3. Results and discussion

3.1 Seven-membered benzothiophene doped with oxygen group elements

Multi-component benzo-based organic semiconductors tend to form large π-conjugated structures with high carrier mobility, and the introduction of thiophene rings improves the performance of the material to a certain extent,[39] so we choose benzothiophene compounds as the research object. Fig. 1 is a schematic diagram of the molecular structure and electron cloud of a seven-membered benzothiophene. It can be seen from Fig. 1b, c and Table S1† that the three sulfur atom electron clouds are densely distributed and the Fukui (−) and Fukui (+) indices have the largest absolute values, indicating that these three sulfur atoms have high activity and are prone to nucleophilic and electrophilic attacks, and they are ideal sites for doping. Therefore, we used sulfur atoms as the starting point[27] to study the effect of doping of oxygen group elements on the performance of organic semiconductors. Next, we conducted mono-, binary-, and ternary doping of the seven-membered benzothiophene with oxygen group elements, and the specific

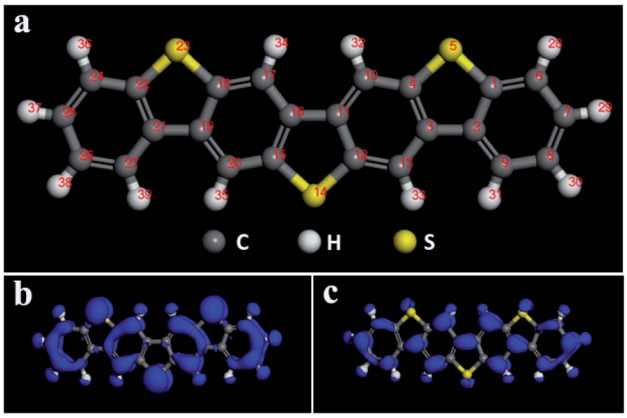

Fig. 1 (a) Schematic diagram of the seven-membered benzothiophene molecular structure; (b) Fukui (−) electron cloud distribution diagram; (c) Fukui (+) electron cloud distribution diagram.

structure is shown in Fig. S1.† According to the symmetry of the molecular structure, both single and binary doping adopt symmetry doping methods to make it more stable. The values of E_{HOMO}, E_{LUMO} and ΔE are used to characterize the ability of the organic semiconductor molecule to bind electrons and the electronic transitions between orbitals. The higher the E_{HOMO}, the stronger the electron donating ability of the molecule, which is conducive to accepting holes; the lower the E_{LUMO}, the better the ability to receive electrons, and the smaller the difference between the two, the faster the electron transfer rate between the orbitals.

It can be seen from Fig. 2, S2, S3 and Table S2† that the doping of Te has greatly changed the E_{HOMO} and E_{LUMO} values of the seven-membered benzothiophene compared to the undoped benzothiopene and that doped with the other oxygen group elements. The ternary Te doping increases the E_{HOMO} value most significantly (0.211 eV), the E_{LUMO} is also reduced and its electron transport is more favorable, it can be seen that Te is a better oxygen doping element. Fig. 3a shows the E_{LUMO}, E_{HOMO}, and ΔE of the undoped and ternary O, Se, and Te-doped seven-membered benzothiophene molecules. As the relative atomic mass of oxygen group elements increases, ΔE gradually decreases. The interelectron transfer rate becomes faster, and the carrier mobility gradually increases. It can be seen from Fig. 3b that when the atoms of the doping site change in the order of O, Se, and Te, their energy values gradually decrease and the changes are more obvious, and the organic semiconductor molecules show a stable trend.

3.2 *o*-Pentacene doped with oxygen group elements

O-Pentacene has a special symmetrical structure with five benzene rings. When doped, the six-membered ring breaks to form a five-membered ring and the molecular structure is shown in Fig. S4.†

It can be seen from Fig. 4, S5, S7 and Table S3† that the decrease in the E_{LUMO} value of the mono Te-doped *o*-pentacene is the most obvious (0.279 eV). The lower the E_{LUMO} value, the stronger the ability of the molecule to receive electrons,

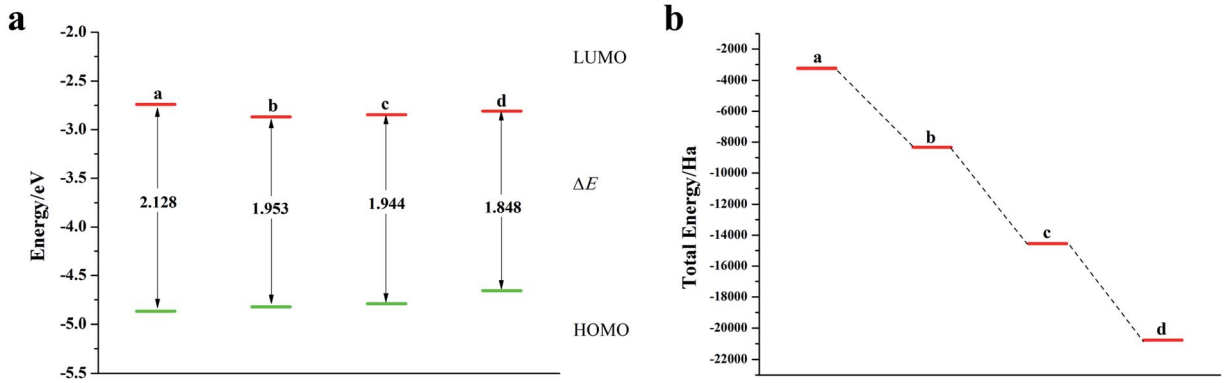

Fig. 2 (a) E_{LUMO}, E_{HOMO}, and ΔE of seven-membered benzothiophene doped with the Te atom; (b) schematic diagram of the total energy of each substance (a: seven-membered benzothiophene; b: mono Te-doped seven-membered benzothiophene; c: binary Te-doped seven-membered benzothiophene; d: ternary Te-doped seven-membered benzothiophene).

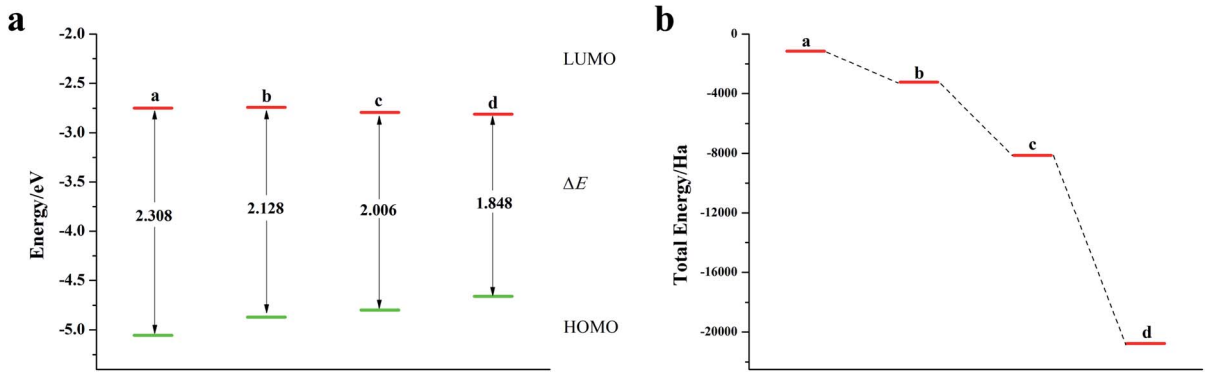

Fig. 3 (a) E_{LUMO}, E_{HOMO}, and ΔE of seven-membered benzothiophene doped with oxygen group elements; (b) schematic diagram of the total energy of each substance (a: ternary O-doped seven-membered benzothiophene; b: seven-membered benzothiophene; c: ternary Se-doped seven-membered benzothiophene; d: ternary Te-doped seven-membered benzothiophene).

indicating that the presence of Te atoms improves the ability of the *o*-pentacene molecule to accept electrons. The binary Te-doped *o*-pentacene (one-five ring) E_{HOMO} value increased by 0.127 eV, indicating that Te doping enhanced the electron donating ability of the molecule. Based on the analysis of E_{HOMO}, E_{LUMO}, ΔE and other data, although the binary Te-doped *o*-pentacene molecule (one-five ring) has better stability, its band gap becomes larger, which is not conducive to electron transport. Doping *o*-pentacene with binary Te (two-four ring) is the best doping method in terms of band gap change and stability. Fig. 5a shows E_{LUMO}, E_{HOMO}, and ΔE of the undoped and mono-O, S, Se, Te doped *o*-pentacene molecules. As the relative atomic mass of oxygen group elements increases, ΔE gradually decreases, the electron transfer rate between E_{HOMO}

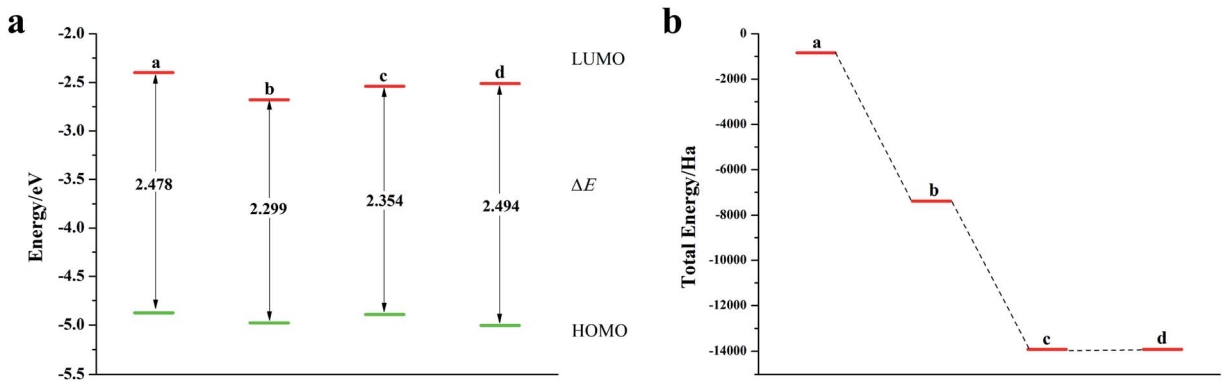

Fig. 4 (a) E_{LUMO}, E_{HOMO}, and ΔE of *o*-pentacene doped with the Te atom; (b) schematic diagram of the total energy of each substance (a: *o*-pentacene; b: mono Te-doped *o*-pentacene; c: binary Te-doped *o*-pentacene (two-four ring); d: binary Te-doped *o*-pentacene (one-five ring)).

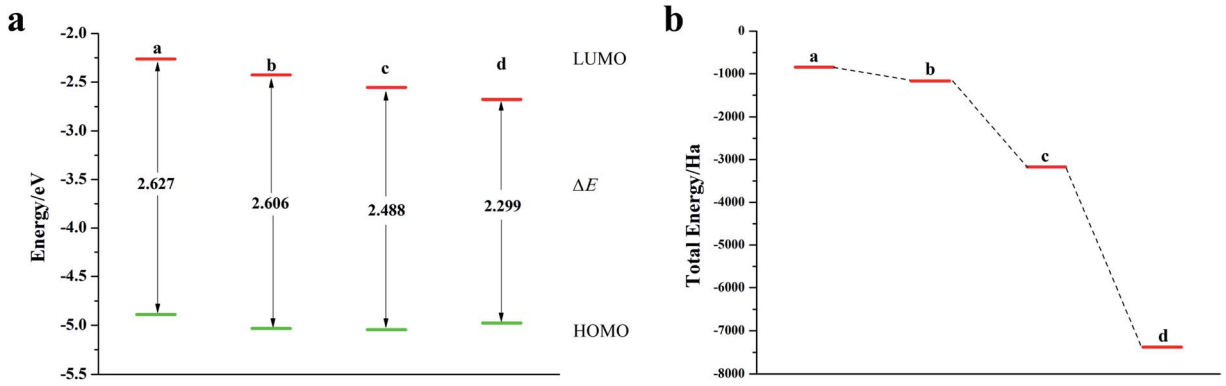

Fig. 5 (a) E_{LUMO}, E_{HOMO} and ΔE of *o*-pentacene doped with oxygen group elements; (b) schematic diagram of the total energy of each substance (a: mono O-doped *o*-pentacene; b: mono S-doped *o*-pentacene; c: mono Se-doped *o*-pentacene; d: mono Te-doped *o*-pentacene).

and E_{LUMO} orbital becomes faster, and the carrier mobility gradually increases. It can be seen from Fig. 5b that when the atoms at the doping site change in the order of O, S, Se, and Te, their energy values gradually decrease and the changes are more obvious, and the organic semiconductor molecules show a stable trend.

3.3 2,6-Diphenyldithiophene (DP-DTT) doped with oxygen group elements

We calculated the Fukui index (Table S4†) of the undoped 2,6-diphenyldithiophene (DP-DTT). The absolute values of the sulfur atoms, Fukui (−) and Fukui (+), are the largest, which

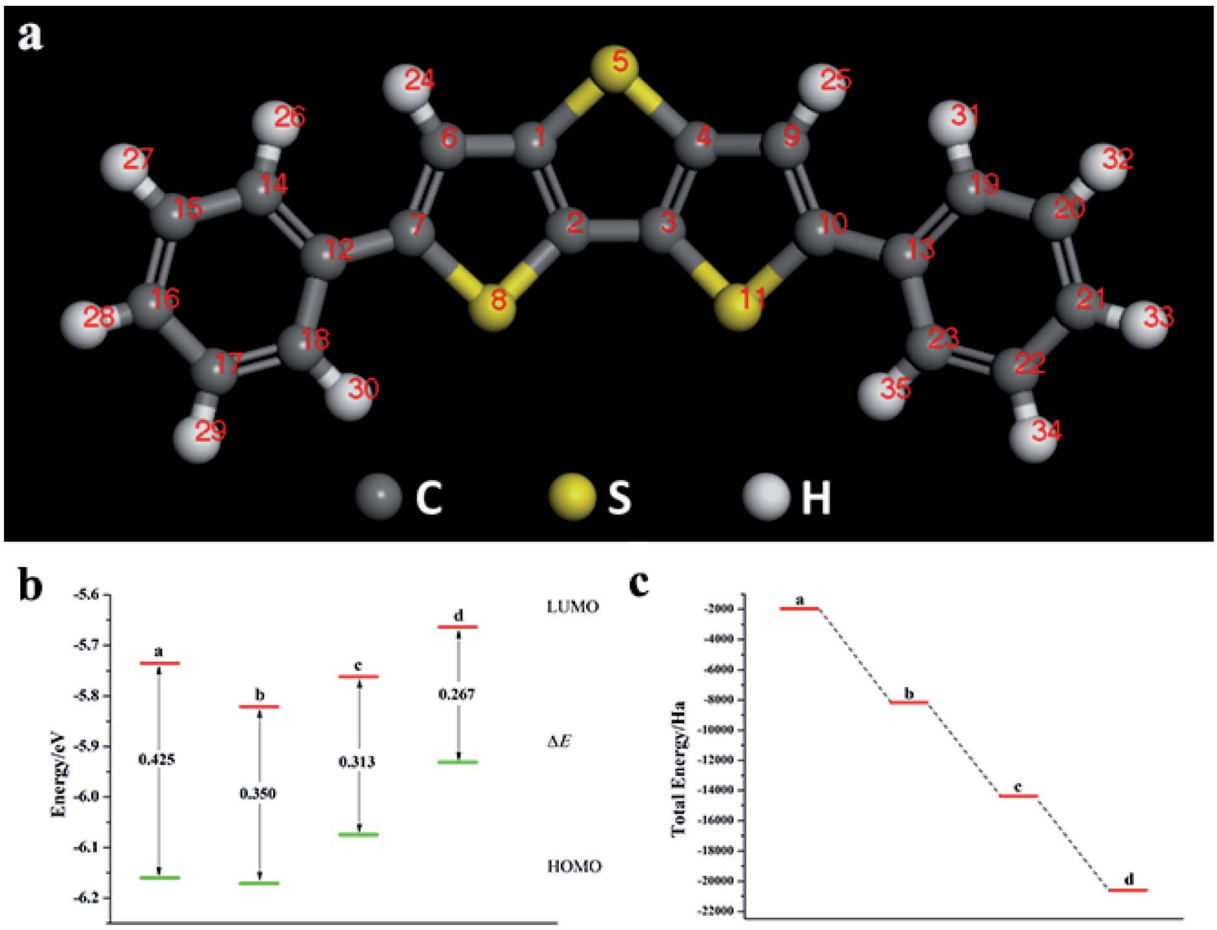

Fig. 6 (a) Schematic diagram of the DP-DTT molecular structure; (b) E_{LUMO}, E_{HOMO}, and ΔE of DP-DTT doped with the Te atom; (c) schematic diagram of the total energy of each substance (a: DP-DTT; b: mono Te-doped DP-DTT; c: binary Te-doped DP-DTT; d: ternary Te-doped DP-DTT).

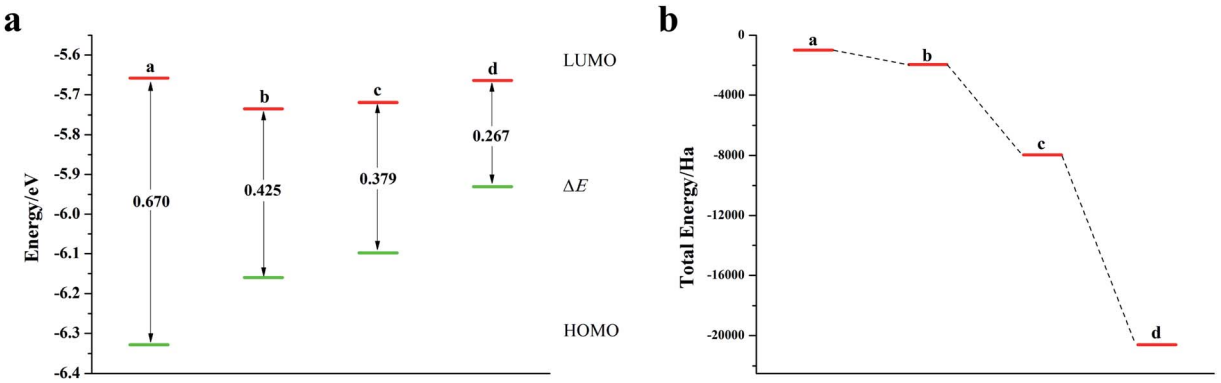

Fig. 7 (a) E_{LUMO}, E_{HOMO}, and ΔE of DP-DTT doped with oxygen group elements; (b) schematic diagram of the total energy of each substance (a: ternary O-doped DP-DTT; b: DP-DTT; c: ternary Se-doped DP-DTT; d: ternary Te-doped DP-DTT).

makes them prone to nucleophilic and electrophilic attacks, and thus they are ideal sites for doping. According to the symmetry of the DP-DTT molecular structure (Fig. 6a), in order to make it more stable, we adopt a symmetrical doping method, and the structural diagram of the doped structure is shown in Fig. S8.†

As can be seen from Fig. 6, S9, S10 and Table S5,† the band gap of DP-DTT molecules becomes smaller and the energy becomes lower after doping with Te atoms. Although the band gap of the ternary Te is the smallest, its E_{LUMO} value is significantly increased, and the decline in the ability to accept electrons is not conducive to electron transport. In contrast, binary

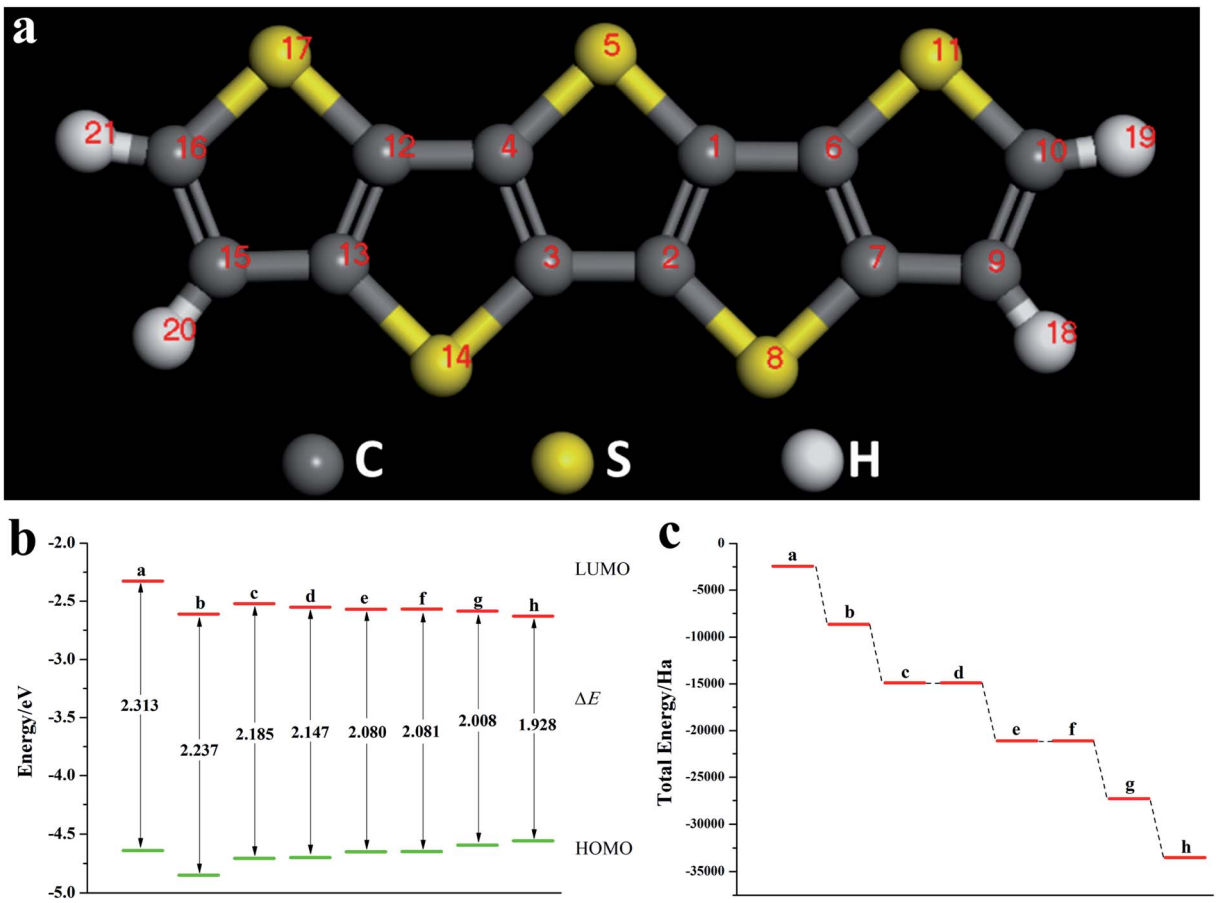

Fig. 8 (a) Schematic diagram of pentacene; (b) E_{LUMO}, E_{HOMO}, and ΔE of pentacene doped with the Te atom; (c) schematic diagram of the total energy of each substance (a: pentacene; b: mono Te-doped pentacene; c: binary Te-doped pentacene (two-four ring); d: binary Te-doped pentacene (one-five ring); e: ternary Te-doped pentacene (two-three-four ring); f: ternary Te-doped pentacene (one-three-five-ring); g: quaternary Te-doped pentacene; h: five membered Te-doped pentacene).

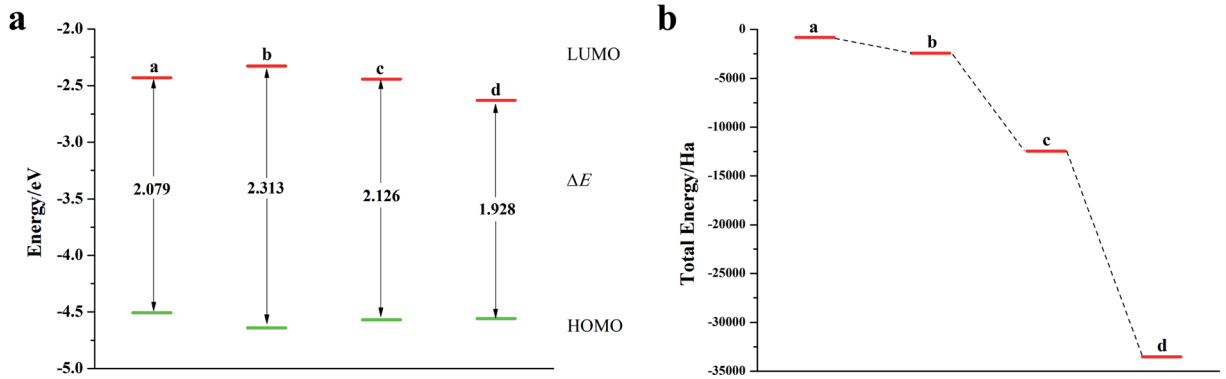

Fig. 9 (a) E_{LUMO}, E_{HOMO} and ΔE of pentacene doped with oxygen group elements; (b) schematic diagram of the total energy of each substance (a: five-membered O doped with pentacene; b: pentacene; c: five Se-doped with pentacene; d: five-membered Te doped with pentacene).

Te doping is an ideal doping method, which not only improves the electron gaining and losing abilities of DP-DTT molecules, but also reduces its band gap. It can be seen from Fig. 7a that when the doped atoms change in the order of O, S, Se, Te, their E_{LUMO} energy values do not change according to a certain law, but the E_{HOMO} value gradually increases with the increase of the relative atomic mass of the oxygen group elements, indicating that its ability to donate electrons is increasing. The band gap width (ΔE) gradually decreases, indicating that the electrons between orbitals easily undergo transitions. It can be seen from Fig. 7b that when the atoms at the doping site change in the order of O, S, Se, Te, their energy values gradually decrease, and the molecules show a stable trend.

3.4 Pentacene doped with oxygen group elements

Fig. 8a is a schematic diagram of the structure of a pentacene molecule; the calculation of the Fukui index (Table S6†) shows that the absolute value of the Fukui index of five sulfur atoms is the largest, indicating that the reaction activity is high and they are ideal doping sites. Next, the pentacene molecule is doped with an oxygen group element, and a schematic diagram of the doped molecular structure is shown in Fig. S11.† According to the symmetry of the molecular structure, the binary oxygen group element is doped into a two-four-ring and one-five-ring, and the ternary oxygen group element is doped into a two-three-four ring and one-three-five ring.

As can be seen from Fig. 8, S12, S13 and Table S7,† the E_{LUMO} value of the mono- and penta-membered Te-doped pentacene decreased the most, being 0.285 eV and 0.302 eV respectively. The quaternary and penta-element Te doping E_{HOMO} values have been increased, and their electron-donating capabilities have been enhanced. With the increase of the number of doping Te atoms, the pentacene molecule shows a stable trend (Fig. 8c), when the number of doping atoms is the same, even if the doping sites are different, they have the same energy. By comparing data such as E_{LUMO}, E_{HOMO}, and ΔE, it was found that the five-membered Te-doped pentacene has a lower E_{LUMO}, higher E_{HOMO}, and smaller band gap, so the best doping method is doping pentacene with five-membered Te. When the doped element changes in the order of S, Se, Te, its E_{LUMO} value gradually decreases, and the E_{HOMO} value changes little, indicating that the doping has little effect on the electron donating ability of the molecule (Fig. 9a). However, the band gap width tends to decrease, which indicates that the electron transfer rate between E_{HOMO} and E_{LUMO} orbitals becomes faster. With the increase of the relative molecular mass of the oxygen group elements (Fig. 9b), the energy value of the organic semiconductor molecule gradually decreases and it is more obvious, showing a stable trend.

4. Conclusion

In summary, through DFT calculations, the influence of doping of oxygen group elements on the properties of four organic semiconductor materials of seven-membered benzothiophene, *o*-pentacene, DP-DTT and pentathiophene is explored. By comparing the changes in molecular data before and after doping, we screened the best doping methods for the four materials, all of which are doped with multi-element Te. It can be seen that Te atom doping can significantly improve the carrier mobility and stability of these four organic semiconductor materials, and the molecular band gaps after doping are reduced by 13.16%, 5.00%, 26.35%, and 16.64%, and the energy value is reduced 5.426 times, 15.45 times, 6.36 times and 12.68 times, respectively. Among them, DP-DTT has the largest decrease in the band gap, indicating that the doping of Te has the greatest effect on its carrier mobility, and *o*-pentacene has the largest decrease in total energy, which proves that the doping of Te atoms has the greatest impact on its stability. By comprehensive comparison, we get the general rule of oxygen group element doping: as the relative atomic mass of oxygen group elements increases, ΔE gradually decreases, and the carrier mobility gradually increases. This research guides experiments from theoretical calculations, provides ideas and directions for specific experimental design, improves the accuracy of research, and accelerates the pace of exploring new organic semiconductor materials.

Conflicts of interest

The authors declare no competing interests.

Acknowledgements

Support of the National Natural Science Foundation of China (21902021, 21908017, 51972293, and 51772039), the Joint Research Fund Liaoning-Shenyang National Laboratory for Materials Science (20180510020), the Fundamental Research Funds for the Central Universities (DUT20RC(4)020 and DUT20RC(4)018), and Supercomputing Center of Dalian University of Technology for this work is gratefully acknowledged.

References

1 A. Facchetti, *Mater. Today*, 2013, **16**, 123–132.
2 H. Huang, L. Yang, A. Facchetti and T. J. Marks, *Chem. Rev.*, 2017, **117**, 10291–10318.
3 K. Eswar Srikanth, K. Ramaiah, D. Jagadeeswara Rao, K. Prabhakara Rao, J. Laxman Naik, A. Veeraiah and J. Prashanth, *Indian J. Phys.*, 2019, **94**, 1153–1167.
4 C. Zhong, C. Duan, F. Huang, H. Wu and Y. Cao, *Chem. Mater.*, 2011, **23**, 326–340.
5 H. D. Pham, H. Hu, F.-L. Wong, C.-S. Lee, W.-C. Chen, K. Feron, S. Manzhos, H. Wang, N. Motta, Y. M. Lam and P. Sonar, *J. Mater. Chem. C*, 2018, **6**, 9017–9029.
6 A. Facchetti, *Chem. Mater.*, 2011, **23**, 733–758.
7 P.-L. T. Boudreault, A. Najari and M. Leclerc, *Chem. Mater.*, 2011, **23**, 456–469.
8 V. Dantanarayana, T. Nematiaram, D. Vong, J. E. Anthony, A. Troisi, K. Nguyen Cong, N. Goldman, R. Faller and A. J. Moule, *J. Chem. Theory Comput.*, 2020, **16**, 3494–3503.
9 F. J. M. Hoeben, P. Jonkheijm, E. W. Meijer and A. P. H. J. Schenning, *Chem. Rev.*, 2005, **105**, 1491–1546.
10 M. Mas-Torrent and C. Rovira, *Chem. Rev.*, 2011, **111**, 4833–4856.
11 H. Sirringhaus, *Adv. Mater.*, 2014, **26**, 1319–1335.
12 S. Holliday, J. E. Donaghey and I. McCulloch, *Chem. Mater.*, 2013, **26**, 647–663.
13 X. Guo, A. Facchetti and T. J. Marks, *Chem. Rev.*, 2014, **114**, 8943–9021.
14 J. Mei, Y. Diao, A. L. Appleton, L. Fang and Z. Bao, *J. Am. Chem. Soc.*, 2013, **135**, 6724–6746.
15 C. B. Nielsen, M. Turbiez and I. McCulloch, *Adv. Mater.*, 2013, **25**, 1859–1880.
16 B. S. Ong, Y. Wu, Y. Li, P. Liu and H. Pan, *Chem.–Eur. J.*, 2008, **14**, 4766–4778.
17 C. Wang, H. Dong, L. Jiang and W. Hu, *Chem. Soc. Rev.*, 2018, **47**, 422–500.
18 A. F. Fernández and K. Zojer, *Appl. Phys. Lett.*, 2017, **111**, 173302.
19 P. V. Pesavento, R. J. Chesterfield, C. R. Newman and C. D. Frisbie, *J. Appl. Phys.*, 2004, **96**, 7312–7324.
20 B. Lüssem, C.-M. Keum, D. Kasemann, B. Naab, Z. Bao and K. Leo, *Chem. Rev.*, 2016, **116**, 13714–13751.
21 Y. Zhang, B. de Boer and P. W. M. Blom, *Adv. Funct. Mater.*, 2009, **19**, 1901–1905.
22 B. Lüssem, M. Riede and K. Leo, *Phys. Status Solidi A*, 2013, **210**, 9–43.
23 C. Mitsui, T. Okamoto, H. Matsui, M. Yamagishi, T. Matsushita, J. Soeda, K. Miwa, H. Sato, A. Yamano, T. Uemura and J. Takeya, *Chem. Mater.*, 2013, **25**, 3952–3956.
24 X. Liu, Y. Liu and Y. Zheng, *Chem. Phys. Lett.*, 2016, **645**, 92–96.
25 A. Putta, J. D. Mottishaw, Z. Wang and H. Sun, *Cryst. Growth Des.*, 2014, **14**, 350–356.
26 J. Hollinger, D. Gao and D. S. Seferos, *Isr. J. Chem.*, 2014, **54**, 440–453.
27 D. Tian, Z. Ma, L. Gu, C. Zhou, C. Li, Z. Wang and H. Wang, *Cryst. Growth Des.*, 2020, **20**, 4479–4490.
28 R. Podeszwa, *J. Chem. Phys.*, 2010, **132**, 044704.
29 J. E. Norton and K. N. Houk, *J. Am. Chem. Soc.*, 2005, 4162–4163.
30 Y. Shirota, *J. Mater. Chem.*, 2000, **10**, 1–25.
31 X. D. Yang, L. J. Wang, C. L. Wang, W. Long and Z. G. Shuai, *Chem. Mater.*, 2008, **20**, 3205–3211.
32 A. Thomas, R. K. Chitumalla, A. L. Puyad, K. V. Mohan and J. Jang, *Comput. Theor. Chem.*, 2016, **1089**, 59–67.
33 S. Yoo, B. Domercq and B. Kippelen, *Appl. Phys. Lett.*, 2004, **85**, 5427–5429.
34 A. L. Appleton, S. M. Brombosz, S. Barlow, J. S. Sears, J.-L. Bredas, S. R. Marder and U. H. F. Bunz, *Nat. Commun.*, 2010, **1**, 1–7.
35 A. N. Sokolov, S. Atahan-Evrenk, R. Mondal, H. B. Akkerman, R. S. Sánchez-Carrera, S. Granados-Focil, J. Schrier, S. C. B. Mannsfeld, A. P. Zoombelt, Z. Bao and A. Aspuru-Guzik, *Nat. Commun.*, 2011, **2**, 1–8.
36 N. L. Janaki, B. Priyanka, A. Thomas and K. Bhanuprakash, *J. Phys. Chem. C*, 2012, **116**, 22663–22674.
37 J. C. S. Costa, R. J. S. Taveira, C. F. R. A. C. Lima, A. Mendes and L. M. N. B. F. Santos, *Opt. Mater.*, 2016, **58**, 51–60.
38 A. M. Liu, X. F. Ren, Q. Y. Yang, J. Sokolowski, J. Guo, Y. Q. Li, L. G. Gao, M. Z. An and G. Wu, *J. Electrochem. Soc.*, 2018, **165**, H725–H732.
39 J. G. Laquindanum, H. E. Katz and A. J. Lovinger, *J. Am. Chem. Soc.*, 1998, **120**, 664–672.